Phonon-Mediated Interlayer Charge Separation and Recombination in a $MoSe_2/WSe_2$ Heterostructure

Zilong Wang,[†,‡] Patrick Altmann,[†] Christoph Gadermaier,[†,¶] Yating Yang,[§] Wei Li,[‖] Lavinia Ghirardini,[†] Chiara Trovatello,[†] Marco Finazzi,[†] Lamberto Duò,[†] Michele Celebrano,[†] Run Long,[§] Deji Akinwande,[‖] Oleg V. Prezhdo,[*,⊥] Giulio Cerullo,[*,†,#] and Stefano Dal Conte[*,†]

†*Dipartimento di Fisica, Politecnico di Milano, Piazza L. da Vinci 32, I-20133 Milano, Italy*

‡*Present affiliation: Department of Physics, Ludwig-Maximilians-Universität München, Am Coulombwall 1, 85748, Garching, Germany*

¶*Center for Nano Science and Technology, Italian Institute of Technology, Via Pascoli 70/3, I-20133 Milano, Italy*

§*College of Chemistry, Key Laboratory of Theoretical and Computational Photochemistry of Ministry of Education, Beijing Normal University, Beijing, P. R. China*

‖*Department of Electrical and Computer Engineering, University of Texas at Austin, Austin, USA*

⊥*Department of Chemistry, University of Southern California, Los Angeles, California 90089, United States*

#*IFN-CNR, Piazza L. da Vinci 32, I-20133 Milano, Italy*

E-mail: prezhdo@usc.edu; giulio.cerullo@polimi.it; stefano.dalconte@polimi.it

Abstract

Monolayer transition metal dichalcogenides bear great potential for photodetection and light harvesting due to their high absorption coefficient. However, these applications require the dissociation of the strongly bound photogenerated excitons. One of the most common ways to achieve this is by vertically stacking two monolayers of different compounds, realizing a band alignment which favors an ultrafast interlayer charge transfer. In such heterostructures, the reported recombination times vary by orders of magnitude and the charge separation and in particular the recombination mechanisms are still elusive. Here we use two color pump-probe microscopy to study the temperature dependent charge separation and recombination processes in a $MoSe_2/WSe_2$ heterostructure. We show that, while the charge separation process is ultrafast ($\sim$200 fs) and virtually temperature independent, the recombination rate increases strongly with temperature. *Ab Initio* quantum dynamics simulations accurately reproduce and rationalize the experiments, indicating that the charge separation is temperature independent because it is barrier-less and involves a dense manifold of acceptor states, being promoted by a relatively high-frequency out-of-plane vibration. The strong temperature dependence of the recombination process, on the other hand, arises from a transient indirect-to-direct bandgap modulation by low frequency shear and layer breathing phonon modes.

Keywords

2D Heterostructure, femtosecond pump-probe spectroscopy, charge transfer, transition metal dichalcogenides, TDDFT.

Semiconducting transition metal dichalcogenides (TMDs) are layered materials in which each layer consists of a hexagonal lattice of transition metal atoms (M, typically Mo or W) embedded between two hexagonal lattices of chalcogen atoms (X, usually S or Se), in MX_2[1] proportions. Since the layers are held together by weak van der Waals interactions, they

can be easily thinned down to a monolayer (ML). The exceptionally high absorption coefficient in TMDs, combined with good chemical stability and a variety of scalable fabrication techniques, hold promise for electronic, optoelectronic, photonic and light-harvesting applications.[2–7] ML-TMDs feature a direct bandgap and their optical properties are dominated by excitons (coulombically bound electron-hole pairs) with large binding energies ($\sim$0.5 eV), promoted by the two-dimensional quantum confinement and by the reduced dielectric screening.

For photodetection and light-harvesting applications it is imperative to efficiently dissociate the photogenerated excitons and to prevent recombination of the charges for a time long enough to extract them from the device or allow them to catalyze a photochemical reaction. While the electrons and holes in indirect bandgap semiconductors quickly relax into separate band extrema with sufficiently different wave vectors to slow down recombination ($\sim$ ns), in direct bandgap semiconductors such as ML-TMDs electron-hole recombination is fast (i.e. few ps at cryogenic temperatures).[8,9] A common solution to prolong carrier lifetime is to interface two different ML-TMDs to form a vertical heterostructure (HS). Since the two materials are held together by weak van der Waals forces, they largely preserve their individual electronic structures. Unlike HS of conventional semiconductors, they do not suffer from lattice mismatch constraints, enabling a very large number of combinations.

Among the different HS, the most interesting for applications are those characterized by a type II, or staggered, band alignment, shown in Fig. 1a, where the valence band maximum and the conduction band minimum lie in different layers.[10–12] This configuration makes it energetically favorable for the photoexcited electrons to be on one semiconductor layer and for the holes to be on the other, promoting ultrafast charge separation.[13–21] Type II HS enable efficient photodetectors,[22] solar cells[23,24] and photocatalysts.[25,26] Upon photoexcitation, intralayer excitons formed in one layer efficiently separate via charge transfer on a sub-ps timescale, resulting in the formation of interlayer (IL) excitons for which the electron and hole reside in different layers. IL excitons are characterized by recombination times several orders

of magnitude longer than the intralayer excitons, up to hundreds of nanoseconds.[27–29] Because of these long recombination times, IL excitons can diffuse over micrometer lengths[30,31] and retain spin/valley polarization, giving rise to pure spin/valley diffusion currents.[32,33] The IL twist angle constitutes an additional tuning knob for IL excitons, as confirmed by the recent observation of Moiré trapped excitons in magic-angle twisted TMD-HS.[34–38]

Time-domain spectroscopies (i.e. transient absorption and time resolved photoluminescence) have been extensively used to study charge separation and recombination dynamics in TMD-HS.[39] Transient absorption experiments performed on HS with different stacking sequences show that the ultrafast separation time τ_S does not depend appreciably on the twist angle $\Delta\phi$ between the crystal axes of the two MLs.[18,19] In contrast, the carrier recombination time τ_R for the $MoSe_2/WSe_2$ HS shows a strong non-monotonous dependence on $\Delta\phi$;[18] however, a systematic study of both the radiative and non-radiative recombination processes and their dependence on $\Delta\phi$, the layer stacking sequence and possibly the dielectric environment of the HS is missing.

IL exciton emission has been mainly studied in the $MoSe_2/WSe_2$ HS showing a progressive intensity quenching and a strong decrease of the decay time upon increasing temperatures.[29] This suggests that the IL recombination process is mainly driven by temperature dependent relaxation channels. IL carrier dynamics has been simulated by different theoretical models,[40–47] predicting an IL charge separation time ranging from few tens of fs to 1-2 ps for different types of HS. Several mechanisms have been proposed to explain the rapid and efficient IL charge transfer in TMD-HS, including the presence of an excitation-induced interfacial dipole,[40] phonon-mediated scattering processes[43,48] and a coherent mixing between donor and acceptor states.[42] On the contrary, a theoretical modelling of the carrier recombination dynamics and an explanation of its temperature dependence are still lacking.

Here we use two-color femtosecond transient absorption microscopy to study the temperature dependence of the charge transfer and recombination dynamics in a $MoSe_2/WSe_2$ HS (see the sketch in Fig. 1a). We time-resolve a nearly temperature independent 200 fs

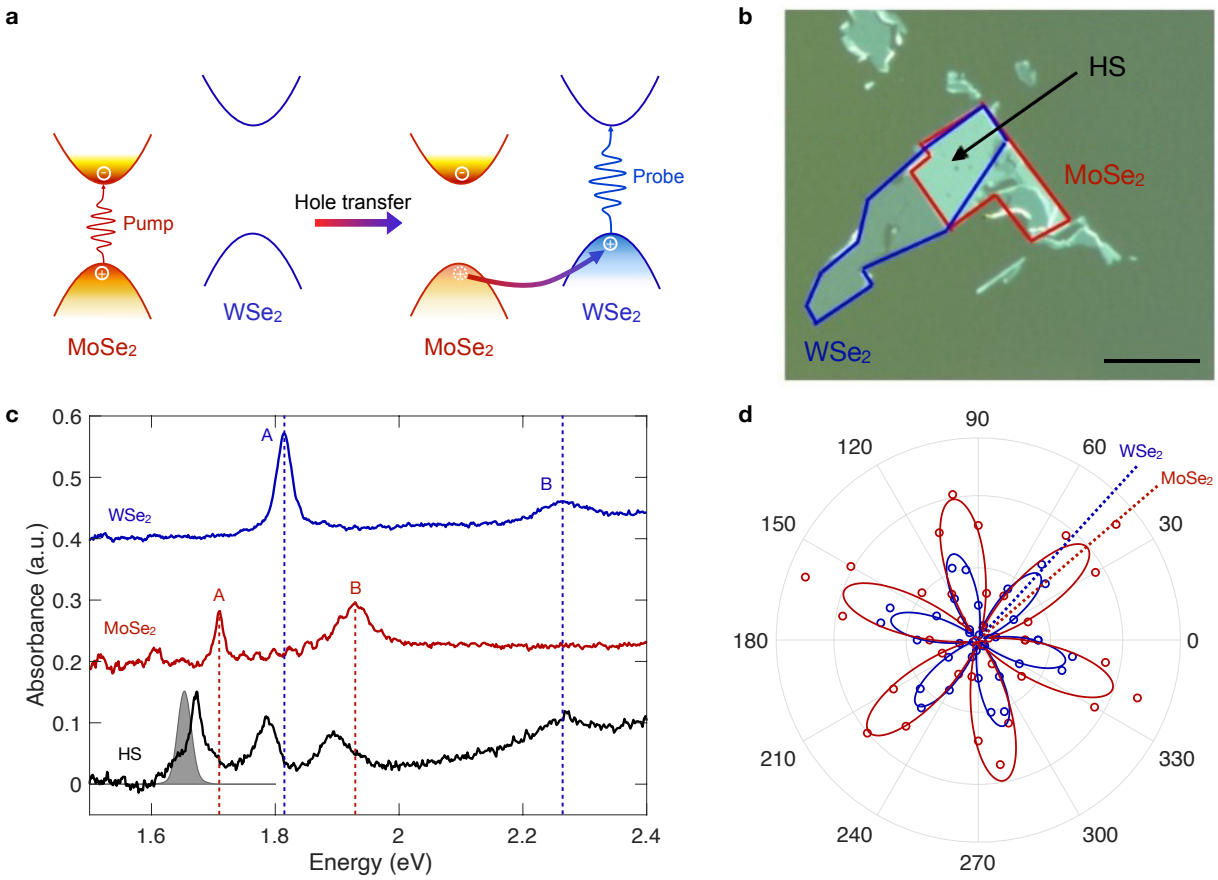

Figure 1: Equilibrium optical properties of the $MoSe_2/WSe_2$ HS. (a) Scheme of the theoretically predicted valence and conduction band alignment at the K/K' points. The arrow represents the IL hole transfer process. (b) Optical microscope image of the HS. The scale bar is 10 µm. (c) Absorption spectra at $T = 9$ K of ML-$MoSe_2$ (red), ML-WSe_2 (blue) and their HS (black). The grey trace is the spectrum of the pump pulse. (d) Angle-dependent second harmonic generation for the evaluation of the twist angle between the layers.

charge separation time and a strongly temperature dependent recombination time, which varies by two orders of magnitude between room temperature and 9K. *Ab Initio* quantum dynamics simulations rationalize our findings, demonstrating that the energy lost during the charge separation and recombination processes is accommodated by the relatively high frequency out-of-plane lattice vibrations, which create a non-adiabatic coupling between the states localized across the interface and cannot be thermally activated within the experimental temperature range. These simulations confirm that the hole transfer is ultrafast and temperature independent, because it is energetically favorable and leads to a dense manifold of acceptor states. On the other hand, the charge recombination process depends on temper-

ature, since it is promoted by heat-activated low frequency shear and layer breathing modes. These phonon modes periodically modulate the band structure of the HS, which bears an indirect gap at equilibrium, and generate a transient direct gap which greatly enhances both the radiative and non-radiative recombination rate of the IL exciton. The unique combination of experiments and *ab Initio* simulations and their very good agreement clarify the microscopic mechanisms underlying the charge separation and recombination processes.

Results and Discussion

The $MoSe_2/WSe_2$ HS, shown in Fig. 1b, was prepared using mechanical exfoliation and transferred onto a fused silica substrate (see Supporting Information). The technique yields ML flakes with a typical lateral size of 30 µm and a ∼10 x 10 µm^2 overlap region when deposited one on top of the other. Figure 1c displays the absorption spectra of the HS and of the individual MLs, measured by white light microscopy at the temperature $T = 9$ K. The MLs show the characteristic A and B absorption resonances ascribed to electronic transitions at the K and K' points, yielding excitons consisting of an electron in the conduction band (CB) and a hole in the spin-orbit split valence band (VB), bound together by Coulomb attraction. $MoSe_2$ has a lower bandgap, with the A exciton peaking at 1.70 eV as compared to 1.81 eV for the A exciton of WSe_2 (see Fig. 1c). The absorption spectrum of the HS shows the A and B resonances of both $MoSe_2$ and WSe_2, including their doping-induced shoulders. All peaks are red shifted compared to their position in the ML, due to the modified dielectric environment.[49] In the HS the A excitonic resonances of $MoSe_2$ and WSe_2 redshift by ∼35 meV and ∼25 meV, respectively. Coupling between the two layers leads to a shift of the band gap and the exciton binding energy via increased dielectric screening, but not to the creation of qualitatively different electronic states around the K and K' points, confirming that the electronic structure of the individual MLs is well retained in the HS due to the weak van der Waals coupling. The twist angle $\Delta\phi$ between the two MLs was measured via

polarization dependent second harmonic generation (SHG) and found to be $\Delta\phi \approx 54^\circ$ (see Fig. 1d and Fig. S4 in the Supporting Information).

To visualize in real time the charge separation and recombination processes in the HS, we employ two-color femtosecond transient absorption microscopy. In this technique the sample is photoexcited by an ultrashort laser pulse (the pump) and the differential transmission ($\Delta T/T$) is measured by a time-delayed laser pulse (the probe) with a different photon energy with respect to the pump. Due to the small size of the HS and to the need to spatially resolve its $\Delta T/T$ signal and distinguish it from those of the neighbouring MLs, pump and probe pulses have been collinearly combined into a home-built microscope (see Fig. S2 in the Supporting Information), allowing a spatial resolution of $\sim 5\,\mu$m.

Figure 2a shows two-color $\Delta T/T$ time traces, measured at $T = 9$ K, with the pump pulse tuned at 1.65 eV, slightly below the $MoSe_2$ A exciton of the HS, and the probe pulse tuned at 1.77 eV, in resonance with the A exciton of WSe_2. Under these conditions only $MoSe_2$ is excited, while the pump photon energy falls below the WSe_2 bandgap. For the $MoSe_2$ ML (red trace in Fig. 2a) we observe a weak negative signal ($\Delta T/T < 0$) which rises instantaneously within the 150 fs instrumental response function (IRF) of the apparatus. Since the 1.77 eV probe photon energy is slightly below the B exciton peak in $MoSe_2$ (located at 1.87 eV), we assign this signal to a rigid red-shift of the B exciton resonance, due to bandgap renormalization (BGR) induced by the carriers photogenerated by the pump pulse.[50] The observation of an instantaneous BGR upon photoexcitation is in agreement with several previous studies on other TMDs.[50,51,53] Moving to the WSe_2 ML (blue trace in Fig. 2a) we observe, except for a weak signal around time zero due to non-resonant pump-probe interactions, no $\Delta T/T$ signal at longer delays; this is expected because the pump photon energy lies well below the bandgap of WSe_2 and the fluence is low enough that multiphoton excitation can be neglected. When moving to the HS (black trace in Fig. 2a) the signal changes dramatically: we observe an intense positive $\Delta T/T$ signal which does not rise instantaneously but with a clearly resolved delay. We interpret this signal as due to Pauli blocking of the A exciton

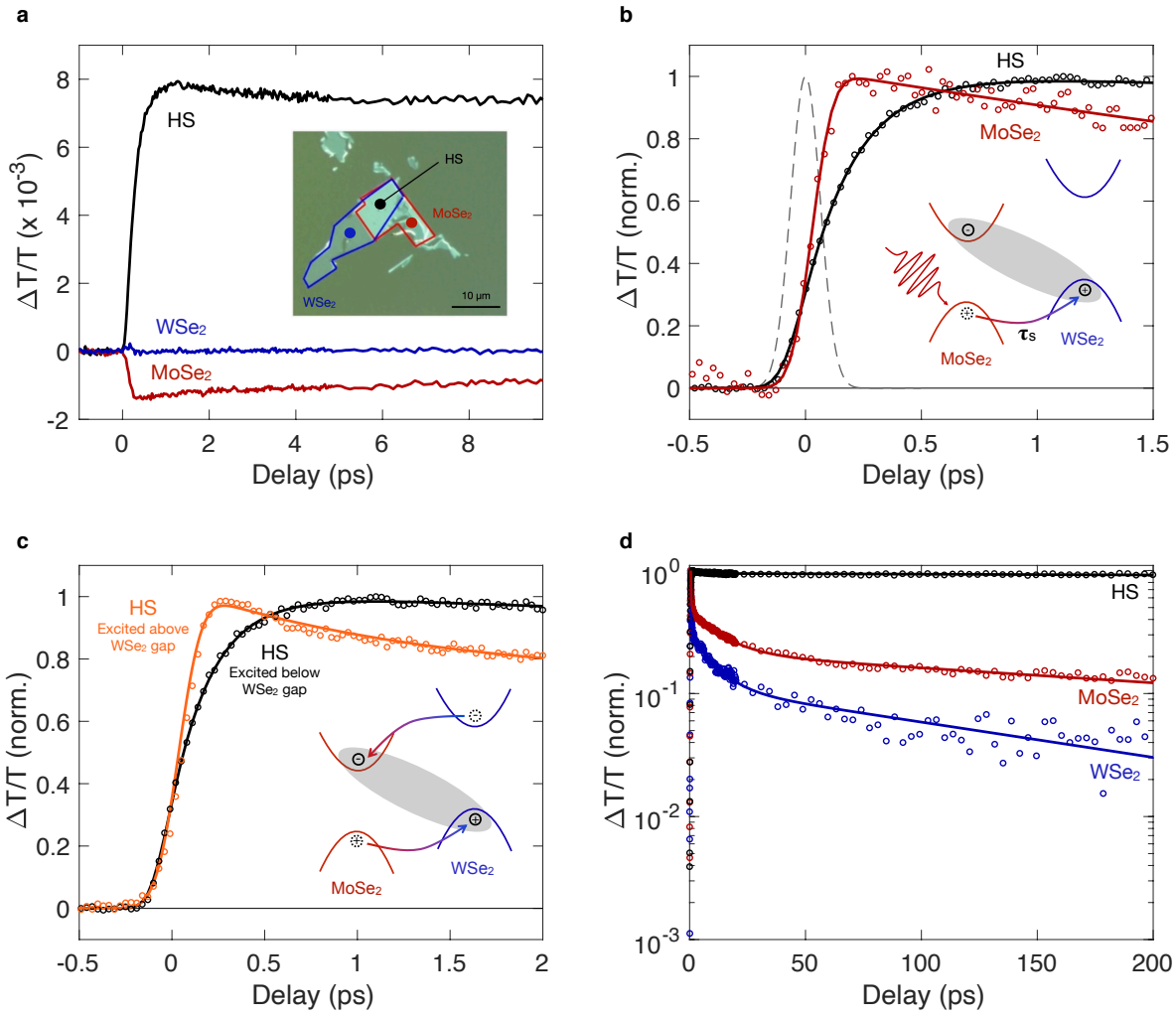

Figure 2: Charge transfer dynamics in $MoSe_2/WSe_2$ HS at $T = 9$ K. (a) $\Delta T/T$ temporal traces measured at the WSe_2 A exciton resonance on the $MoSe_2/WSe_2$ HS (black) and the isolated $MoSe_2$ (red), WSe_2 (blue) layers, upon optical excitation resonant with the optical band gap of $MoSe_2$ (1.69 eV). The incident pump fluence is 70 $\frac{\mu J}{cm^2}$. (b) Comparison between the build-up dynamics of the $\Delta T/T$ traces of the HS and $MoSe_2$ (both traces are normalized for a better comparison). The maximum variation of the signal measured on the HS is clearly delayed with respect to the one of the $MoSe_2$ because of the finite hole transfer time. The continuous lines are fits to the data. (c) Comparison between $\Delta T/T$ response of the HS for layer (black) and non layer-selective (orange) photo-excitation (i.e. pump energy below (1.69 eV) and above (2.07 eV) the optical gap of $MoSe_2$). In the latter case, the signal exhibits an instantaneous build-up time as for the isolated TMD layers. (d) Long delay dynamics at the energy of the WSe_2 A exciton measured on the HS excited with pump photon energy of 1.69 eV compared with the A exciton resonance measured on the isolated $MoSe_2$ and WSe_2 layers (pump photon energy at 2.07 eV). Continuous lines are fits to the data with a double exponential decay function. The longer decay constant extracted from the fit is 470 ps ($MoSe_2$) and 180 ps (WSe_2), while it becomes >3 ns for the HS.

transition in WSe_2 from holes in the VB of WSe_2, which have been injected following charge transfer from the VB of $MoSe_2$ and IL exciton formation.

Figure 2b compares the normalized $\Delta T/T$ dynamics for $MoSe_2$ and for the HS, measured at $T = 9$ K. In order to visually capture their different build-up times the $MoSe_2$ dynamics has been flipped in sign. It is evident that the HS signal has a delayed build-up which is well resolved by our experiment; fitting the process with an exponential rise, convoluted with the IRF (i.e. the cross-correlation of the pump and probe pulses intensity profiles, with a full width at half maximum of 150 fs) yields a time constant $\tau_S = 200 \pm 20$ fs for the charge separation process. This result is in a good agreement with previous studies on similar TMD HS, which found τ_S of the same order of magnitude and showed it to be independent of twist angle.[18] By tuning the pump photon energy above the optical gap of WSe_2, the $\Delta T/T$ signal (orange curve in Fig. 2c) shows a pulse-width limited build-up dynamics, comparable to the one measured in the isolated TMD layers. The change of the rise time is a consequence of the lack of layer selectivity for the photo-excitation: at increasing pump photon energy the pump pulse creates excitons also in the WSe_2 layer of the HS. This results in an instantaneous bleaching signal measured at A excitonic transition of WSe_2. Creation of intralayer excitons in both the TMD layers opens up new scattering channels for the photoexcited carriers, giving rise to a fast electron transfer from WSe_2 to $MoSe_2$ resulting in a sub-picosecond decay component.

Figure 2d shows the dynamics of the HS at 9 K on a longer timescale. The positive $\Delta T/T$ signal shows an initial decay by few percent on a few-ps timescale, followed by a slow exponential decay with a time constant τ_R of several ns. As a comparison, we show the decay of the A exciton photobleaching signal in ML-WSe_2 when the photoexcitation is tuned above its bandgap to 2.07 eV (blue line in Fig. 2d); in this case the signal features a much faster and multi-exponential decay. As expected, the IL excitons in the HS recombine much more slowly than the intralayer excitons in the ML.[14,27]

Having identified a clear spectral signature of the IL exciton dynamics in the HS, we set

out to investigate the temperature dependence of its formation and decay processes. Figure 3a compares the IL exciton build-up process measured at 9 K and at RT; the dynamics appear similar, with only a slight speed-up observed in the RT data. This is confirmed by performing a temperature dependence of the IL exciton formation process and extracting an charge separation time constant τ_S (Fig. 3c) which is nearly independent of temperature. We stress that such temperature-independent τ_S has been previously observed in a WS_2/WSe_2 HS and found to be shorter than the 60 fs time resolution of the setup used for that study.[52] Figure 3b reports the temperature dependence of the IL exciton recombination process, measured up to 200 ps timescale due to experimental limitations. We stress that for all the temperature range explored in the experiment, a double exponential decay model provides a better fit to the dynamics than a single exponential one. While the fast decay component slightly depends on the temperature, the slower one (τ_R) displays a stronger dependence with the temperature going from τ_R =5±0.4 ns at 9 K to τ_R =80±10 ps at RT. Figure 3d shows the time constants extracted from the fit of the time traces. The strong temperature dependence of τ_R is related to the drastic reduction of the IL exciton radiative recombination time, previously observed with time-resolved photoluminescence on the same type of HS and not understood.[28,29]

In order to rationalize the observed temperature dependences of the IL exciton formation and recombination processes, we carried out *Ab Initio* quantum dynamics simulations combining real-time time-dependent density functional theory and non-adiabatic molecular dynamics.[54–56] The simulations are performed on the $MoSe_2/WSe_2$ HS shown in Fig. 4. The band structure calculations show, in agreement with previous results,[57,58] that the $MoSe_2/WSe_2$ HS has an indirect bandgap. Because the $MoSe_2$ VB maximum (VBM) is inside the WSe_2 VB, the $MoSe_2$ VBM couples and mixes with multiple WSe_2 states (see Fig. 4c), such that the initial state for the hole transfer process can be delocalized between the two layers, facilitating ultrafast charge transfer across the weakly coupled van der Waals HS.[42,59] Figure 5a shows the calculated build-up of the hole population in WSe_2,

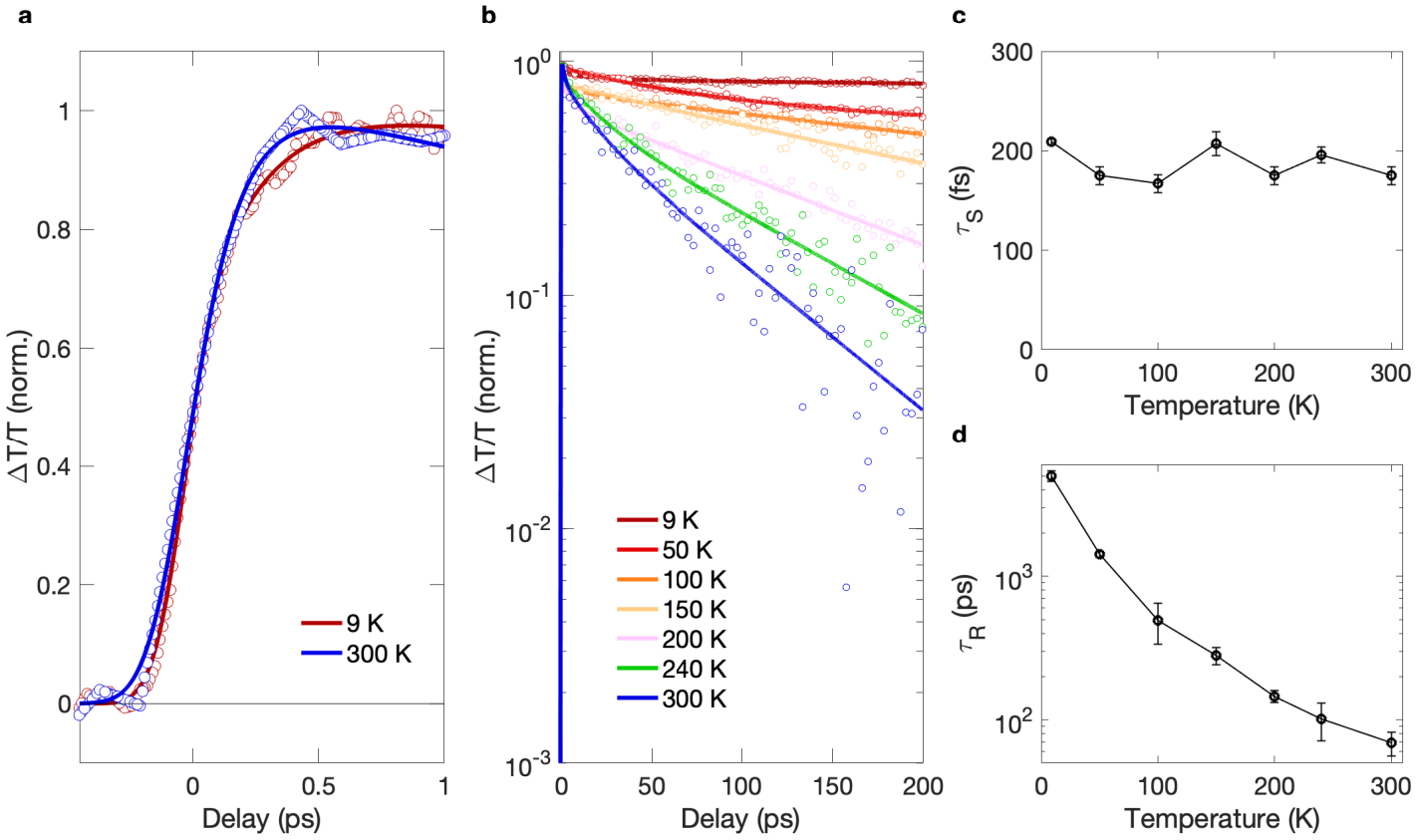

Figure 3: Temperature dependent exciton dissociation and recombination dynamics. (a) Early delay time $\Delta T/T$ dynamics measured on the HS for pump at 1.67 eV and probe at 1.78 eV for different sample temperatures (open symbols) and fits of the build-up dynamics (continuous lines). (b) Relaxation dynamics measured at different temperatures (open symbols) and fits to a double-exponential decay (continuous lines). (c) Charge separation time extracted from the fit function in (a) at different temperatures. (d) τ_R as a function of the temperature. τ_R is the longer decay constant extracted from a double exponential fit of the temporal traces.

following selective excitation of $MoSe_2$. The hole transfer is ultrafast and independent of temperature (see Fig. 5b), because it is energetically favorable and is characterised by a high density of final states in the dense manifold of WSe_2 VB states, and since it is promoted by TMDs out-of-plane motions[60] with frequencies around 240-250 cm^{-1} (see Fig. S5a in the Supporting Information). Phonons at such frequencies cannot be thermally activated within the experimental temperature range, since 250 cm^{-1} corresponds to ~360 K in agreement with the observed temperature independence of the charge separation process. Rapid non-adiabatic transition from the $MoSe_2$ VBM to WSe_2 VB states immediately below in

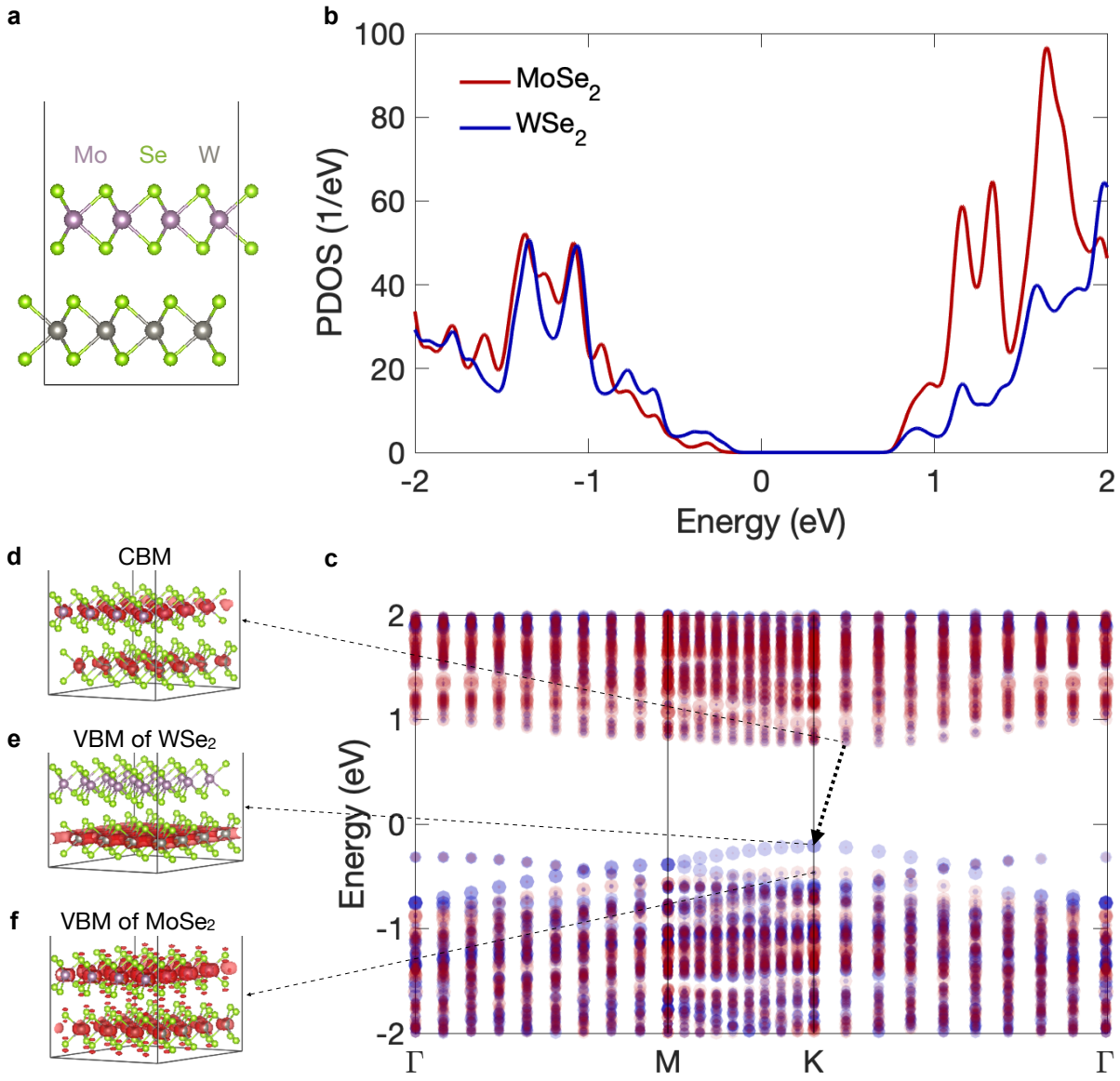

Figure 4: Simulated $MoSe_2/WSe_2$ HS and its electronic properties. (a) Geometric structure of the simulation cell. (b) Projected density of states (PDOS) of the $MoSe_2/WSe_2$ HS obtained with PBE+SOC. 30 k-points from Γ to M to K to Γ are sampled with 10 k-points between each pair. (c) Projected band structure corresponding to the PDOS in part (b). The arrow indicates the indirect bandgap. (d), (e), (f) Charge densities for conduction band minimum (CBM), valence band maximum (VBM) of WSe_2 and VBM of $MoSe_2$, respectively.

energy localizes the holes within WSe_2, resulting in an ultrafast transfer. Longer timescale *Ab Initio* quantum dynamics simulations, Fig. 5c-d, also support the experimental results for the IL exciton recombination. Similar to the experiments, the simulations show a strong temperature dependence of the charge recombination, with the timescale ranging from over

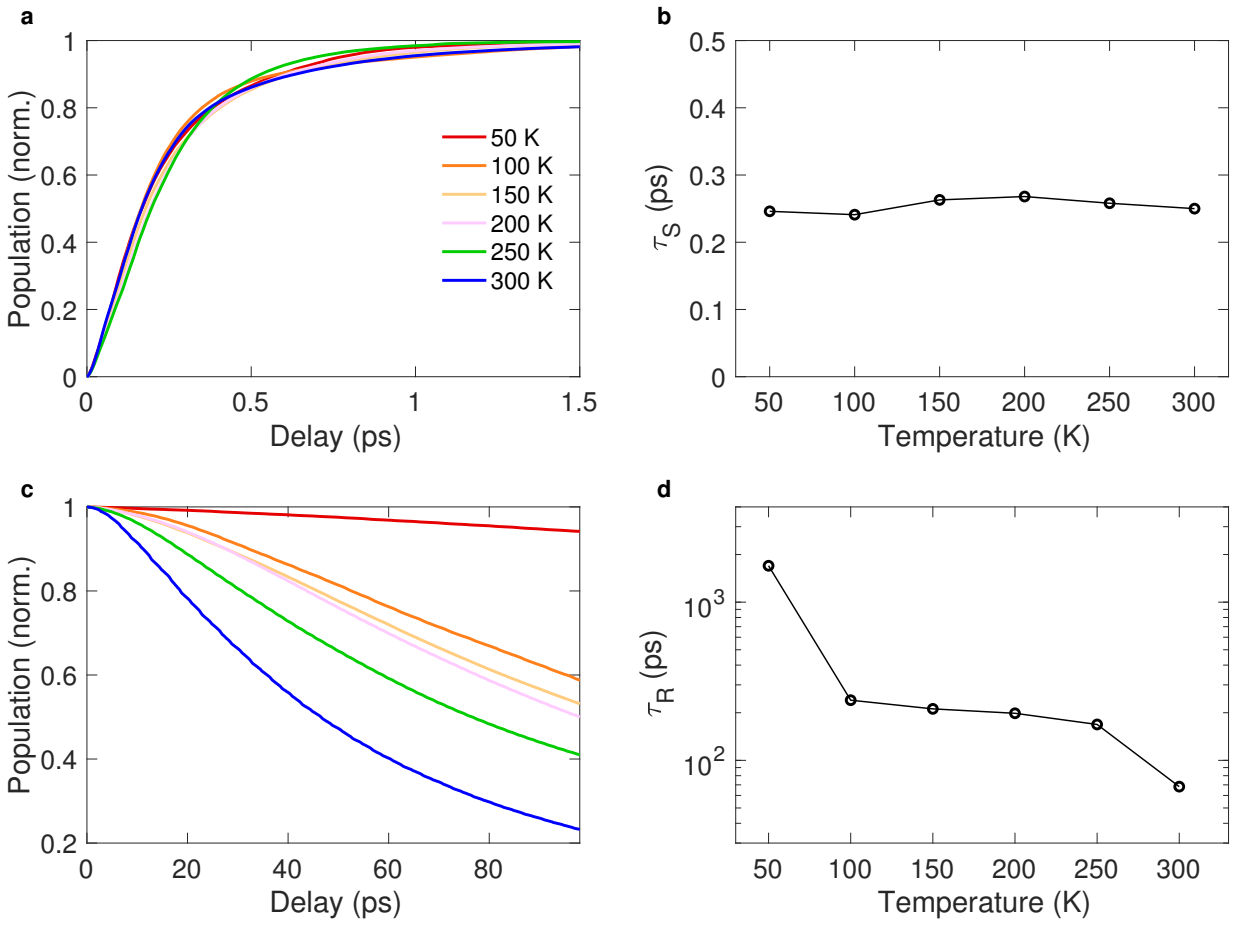

Figure 5: *Ab Initio* nonadiabatic molecular dynamics of charge separation and recombination in the $MoSe_2/WSe_2$ HS. (a) Evolution of hole population on the WSe_2 layer at different temperatures. (b) Hole transfer time vs. temperature. Hole transfer is rapid and independent of temperature because it occurs within a dense manifold of states and is driven by the same high frequency phonon, Fig S2. (c) Decay of population of the IL exciton over time due to nonradiative electron-hole recombination at different temperatures. The decay slows down considerably at lower temperatures due to decreased non-adiabatic electron-phonon coupling and increased band gap, Table S1. (d) Temperature dependence of the calculated recombination time.

1 ns at 50 K, to under 100 ps at 300 K (see Table S1 in the Supporting Information). Just as for the hole transfer, the electronic energy lost during the recombination is deposited into the out-of-plane TMD motions in the 240-250 cm^{-1} frequency range (Fig. S5b in the Supporting Information). These modes cannot be thermally activated within the considered temperature range, and therefore, the temperature dependence arises from another source.

In particular, the $MoSe_2/WSe_2$ HS has an indirect bandgap (see Fig. 4c), but the energy difference to the direct bandgap is small, around 10 meV. The atomistic simulations show that low frequency motions of the $MoSe_2/WSe_2$ HS, such as the shear (18 cm^{-1}) and layer breathing (29 cm^{-1}) modes,[60] perturb the bilayer geometry, frequently turning it into a direct bandgap material and allowing charge recombination without a variation of crystal momentum. These slow vibrations, with frequencies corresponding to 25-40 K, are activated thermally within the studied temperature range, rationalizing the observed behavior. Contrary to its strong temperature dependence, τ_R is largely independent of the excitation fluence (see Fig. S3 in the Supporting Information) and hence of the exciton or charge density. This suggests that the electron-hole pair after separation remain paired in an IL exciton and eventually recombine with each other (geminate recombination), resulting in dynamic behavior that is independent of the excitation density. If, on the other hand, the separated charges diffused inside the MLs until a non-geminate recombination occurs, one would instead observe a higher recombination rate for higher excitation fluences. This fluence independence confirms our assignment of τ_R to the IL exciton recombination and rules out the most important alternative assignments. Our data show that a significant fraction of all initially excited carriers recombines via this process, which dominates the dynamics in the temporal window between 30 and 200 ps. This does not, however, exclude the presence of other recombination pathways, which may even be dominant on a slower timescale. Both the Shockley-Read-Hall mechanism and Auger recombination[24,61] would display only a weak temperature dependence and a decreasing recombination rate at higher fluences. Similarly, we can exclude the dominant role of dark excitons in the recombination dynamics because they would give rise to a recombination rate decreasing with temperature, as observed in Se-based TMDs, where dark excitons are energetically lower lying with respect to the bright ones.[62]

Conclusions

In conclusion, we have employed ultrafast transient absorption microscopy to study the temperature dependent IL charge separation and recombination process in a $MoSe_2/WSe_2$ HS. We have resolved the charge separation dynamics with a time constant $\tau_S = 200 \pm 20$ fs and found that this time constant is virtually independent of temperature. On the other hand, the recombination time constant τ_R displays a strong temperature dependence, becoming progressively shorter at higher temperatures. *Ab Initio* quantum dynamics simulations reproduce the experimental data very well and shed light on the underlying physical processes. They demonstrate that the energy lost by the charges during the photo-induced charge separation and recombination is accommodated by the relatively high frequency out-of-plane TMD vibrations that create a nonadiabatic coupling between the states localized across the interface. Since the activation temperature of these phonon modes is higher than the experimental temperature range, the hole transfer process is temperature independent. The charge recombination, on the other hand, depends on temperature, because thermally-activated low-frequency phonon modes transiently modulate the system geometry and bring the heterojunction from an indirect bandgap to a direct bandgap, allowing recombination without variation of crystal momentum. The good agreement between theory and experiment allows us to generalize our approach to other materials and indicates that the time-domain simulations can be used to design novel HS with higher charge separation efficiency and improved performances.

Acknowledgements

We acknowledge funding from PRIN 2017 Programme (Prot. 20172H2SC4) from the MIUR, PRIN 2017 NOMEN (Prot. 2017MP7F8F), the support by the European Union Horizon 2020 Programme under Grant Agreement No. 881603 Graphene Core 3 and the support of the US National Science Foundation Grant CHE-1900510. D.A. acknowledges the Presidential

Early Career Award for Scientists and Engineers (PECASE) Grant No W911NF-16-1-0277.

References

(1) Chhowalla, M.; Shin, H. S.; Eda, G.; Li, L.-J., Loh, K. P.; Zhang, H. The Chemistry of Two-Dimensional Layered Transition Metal Dichalcogenide Nanosheets. *Nat. Chem.*, **2013**, *5*, 263-275.

(2) Radisavljevic, B.; Radenovic, A.; Brivio, J.; Giacometti, V.; Kis, A. Single-Layer MoS_2 Transistors. *Nat. Nanotechnol.*, **2011**, *6*, 147-150.

(3) Wang, Q. H.; Kalantar-Zadeh, K.; Kis, A.; Coleman, J. N.; Strano, M. S. Electronics and Optoelectronics of Two-Dimensional Transition Metal Dichalcogenides. *Nat. Nanotechnol.*, **2012**, *7*, 699-712.

(4) Fiori, G.; Bonaccorso, F.; Iannaccone, G.; Palacios, T.; Neumaier, D.; Seabaugh, A.; Banerjee, S. K.; Colombo, L. Electronics Based on Two-Dimensional Materials. *Nat. Nanotechnol.*, **2014**, *9*, 768-779.

(5) Jariwala, D.; Sangwan, V. K.; Lauhon, L. J.; Marks, T. J.; Hersam, M. C. Emerging Device Applications for Semiconducting Two-Dimensional Transition Metal Dichalcogenides. *ACS Nano*, **2014**, *8*, 1102-1120.

(6) Mak, K. F.; Shan, J. Photonics and Optoelectronics of 2D Semiconductor Transition Metal Dichalcogenides. *Nat. Photonics*, **2016**, *10*, 216-226.

(7) Koppens, F. L. H.; Mueller, T.; Avouris, Ph.; Ferrari, A. C.; Vitiello, M. S.; Polini, M. Photodetectors based on graphene, other two-dimensional materials and hybrid systems. *Nat. Nanotechnol.*, **2014**, *9*, 780-793.

(8) Palummo, M.; Bernardi, M.; Grossman, J. Exciton radiative lifetimes in two-dimensional transition metal dichalcogenides. *Nano Lett.*, **2015**, *15*, 2794–2800.

(9) Robert, C.; Lagarde, D.; Cadiz, F.; Wang, G.; Lassagne, B.; Amand, T.; Balocchi, A.; Renucci, P.; Tongay, S.; Urbaszek, B.; Marie, X. Exciton radiative lifetime in transition metal dichalcogenide monolayers. *Phys. Rev. B*, **2016**, *93*, 205423.

(10) Komsa, H.-P.; Krasheninnikov A. V. Electronic structures and optical properties of realistic transition metal dichalcogenide heterostructures from first principles. *Phys. Rev. B*, **2013**, *88*, 085318.

(11) Amin, B.; Singh, N.; Schwingenschlögl, U. Heterostructures of transition metal dichalcogenides. *Phys. Rev. B*, **2015**, *92*, 075439.

(12) Wu, D.; Li, W.; Rai, A.; Wu, X.; Movva, H. C. P.; Yogeesh, M. N.; Chu, Z.; Banerjee, S. K.; Akinwande, D.; Lai, K. Visualization of Local Conductance in MoS_2/WSe_2 Heterostructure Transistors. *Nano Lett.*, **2019**, *19*, 1976–1981.

(13) Hong, X.; Kim, J.; Shi, S.-F.; Zhang, Y.; Jin, C.; Sun, Y.; Tongay, S.; Wu, J.; Zhang Y.; Wang, F. Ultrafast Charge Transfer in Atomically Thin MoS_2/WS_2 Heterostructures. *Nat. Nanotechnol.*, **2014**, *9*, 682–686.

(14) Ceballos, F.; Bellus, M. Z.; Chiu, H.-Y.; Zhao, H. Ultrafast Charge Separation and Indirect Exciton Formation in a MoS_2-$MoSe_2$ Van Der Waals Heterostructure. *ACS Nano*, **2014**, *8*, 12717–12724.

(15) Pan, S.; Ceballos, F.; Bellus, M. Z.; Zereshki, P.; Zhao, H. Ultrafast charge transfer between $MoTe_2$ and MoS_2 monolayers. *2D Mater.*, **2016**, *4*, 015033.

(16) Ceballos, F.; Ju, M.-G-; Lane, S. D.; Cheng Zeng, X.; Zhao, H. Highly Efficient and Anomalous Charge Transfer in van der Waals Trilayer Semiconductors. *Nano Lett.*, **2017**, *17*, 1623–1628.

(17) Xu, W.; Liu, W.; Schmidt, J.F.; Zhao, W.; Lu, X.; Raab, T.; Diederichs, C.; Gao,

W.; Seletskiy, D.V.; Xiong, Q. Correlated fluorescence blinking in two-dimensional semiconductor heterostructures. *Nature*, **2017**, *541*, 62–67.

(18) Zhu H.; Wang, J.; Gong, Z.; Kim Y.D.; Hone, J.; and Zhu, X.-Y. Interfacial Charge Transfer Circumventing Momentum Mismatch at Two-Dimensional van der Waals Heterojunctions. *Nano Lett.*, **2017**, *17*, 3591–3598.

(19) Ji, Z.; Hong, H.; Zhang J.; Zhang, Q.; Huang, W.; Cao, T.; Qiao, R.; Liu, C.; Liang, J.; Jin, C.; Jiao, L.; Shi, K.; Meng, S.; Liu, K. Robust Stacking-Independent Ultrafast Charge Transfer in MoS_2/WS_2 bilayers. *ACS Nano*, **2017**, *11*, 12020–12026.

(20) Jin, C.; Ma, E. Y.; Karni, O.; Regan, E. C.; Wang, F.; Heinz, T. F. Ultrafast Dynamics in Van Der Waals Heterostructures. *Nat. Nanotechnol.*, **2018**, *13*, 994–1003.

(21) Liu, F.; Li, Q.; Zhu, X.-Y. Direct determination of momentum-resolved electron transfer in the photoexcited van der Waals heterobilayer WS_2/MoS_2. *Phys. Rev. B*, **2020**, *101*, 201405(R).

(22) Cheng, R.; Li, D.; Zhou, H.; Wang, C.; Yin, A.; Jiang, S.; Liu, Y.; Chen, Y.; Huang, Y.; Duan, X. Electroluminescence and Photocurrent Generation From Atomically Sharp WSe_2/MoS_2 heterojunction p–n diodes. *Nano Lett.*, **2014**, *14*, 5590–5597.

(23) Pospischil, A.; Furchi, M. M.; Mueller, T. Solar-Energy Conversion and Light Emission in an Atomic Monolayer p–n Diode. *Nature Nanotech.*, **2014**, *9*, 257–261.

(24) Lee, C.-H.; Lee, G.-H.; van der Zande, A. M.; Chen, W.; Li, Y.; Han, M.; Cui, X.; Arefe, G.; Nuckolls, C.; Heinz, T. F.; Guo, J.; Hone, J.; Kim, P. Atomically Thin p–n Junctions with Van Der Waals Heterointerfaces. *Nature Nanotech.*, **2014**, *9*, 676–681.

(25) Shi, J.; Tong, R.; Zhou, X.; Gong, Y.; Zhang, Z.; Ji, Q.; Zhang, Y.; Fang, Q.; Gu, L.; Wang, X.; Liu, Z.; Zhang, Y. Temperature-Mediated Selective Growth of MoS_2/WS_2

and WS_2/MoS_2 Vertical Stacks on Au Foils for Direct Photocatalytic Applications. *Adv. Mater.*, **2016**, *28*, 10664–10672.

(26) Pesci, F. M.; Sokolikova, M. S.; Grotta, C.; Sherrell, P. C.; Reale, F.; Sharda, K.; Ni, N.; Palczynski, P.; Mattevi, C. MoS_2/WS_2 Heterojunction for Photoelectrochemical Water Oxidation *ACS Catal.*, **2017**, *78*, 4990–4998.

(27) Rivera, P.; Schaibley, J. R.; Jones, A. R.; Ross, J. S.; Wu, S.; Aivazian, G.; Klement, P.; Seyler, K.; Clark, G.; Ghimire, N. J.; Yan, J.; Mandrus, D. G.; Yao, W.; Xu, X. Observation of Long-Lived Interlayer Excitons in Monolayer $MoSe_2/WSe_2$ Heterostructures *Nat. Commun.*, **2015**, *6*, 6242.

(28) Miller, B.; Steinhoff, A.; Pano, B.; Klein, J.; Jahnke, F.; Holleitner, A.; Wurstbauer, U. Long-Lived Direct and Indirect Interlayer Excitons in van der Waals Heterostructures. *Nano Lett.*, **2017**, *17*, 5229–5237.

(29) Nagler, P.; Plechinger, G.; Ballottin, M.V.; Mitioglu, A.; Meier, S.; Paradiso, N.; Strunk, C.; Chernikov, A.; Christianen, P.C.M.; Schüller, C.; Korn, T. Interlayer Exciton Dynamics in a Dichalcogenide Monolayer Heterostructure. *2D Mater.*, **2017**, *4*, 025112.

(30) Unuchek, D.; Ciarrocchi, A.; Avsar, A.; Watanabe, K.; Taniguchi, T.; Kis, A. Room-Temperature Electrical Control of Exciton Flux in a van der Waals Heterostructure. *Nature*, **2018**, *560*, 340–344.

(31) Yuan, L.; Zheng, B.; Kunstmann, J.; Brumme, T.; Kuc, A. B.; Ma, C.; Deng, S.; Blach, D.; Pan, A.; Huang, L. Twist-Angle-Dependent Interlayer Exciton Diffusion in WS_2–WSe_2 heterobilayers *Nat. Mater.*, **2020**, *19*, 617–623.

(32) Jin, C.; Kim, J.; Iqbal Bakti Utama, M.; Regan, E. C.; Kleemann, H.; Cai, H.; Shen, Y.; Shinner, M. J.; Sengupta, A.; Watanabe, K.; Taniguchi, T.; Tongay, S.;

Zettl, A.; Wang, F. Imaging of Pure Spin-Valley Diffusion Current in WS_2-WSe_2 Heterostructures. *Science*, **2018**, *360*, 893–896.

(33) Unuchek, D.; Ciarrocchi, A.; Avsar, A.; Sun, Z.; Watanabe, K.; Taniguchi, T.; Kis, A. Valley-polarized Exciton Currents in a van der Waals Heterostructure. *Nat. Nanotech.*, **2019**, *14*, 1104–1109.

(34) Zhang, N.; Surrente, A.; Baranowski, M.; Maude, D. K.; Gant, P.; Castellanos-Gomez, A.; Plochocka P. Moiré Intralayer Excitons in a $MoSe_2/MoS_2$ Heterostructure. *Nano Lett.*, **2018**, *18*, 7651–7657.

(35) Seyler, K.L.; Rivera, P.; Yu, H.; Wilson, N.P.; Ray, E.L.; Mandrus, D.G.; Yan, J.; Yao, W.; Xu, X. Signatures of Moiré-trapped Valley Excitons in $MoSe_2/WSe_2$ Heterobilayers. *Nature*, **2019**, *567*, 66–70.

(36) Tran, K.; *et al.* Evidence for Moiré excitons in van der Waals Heterostructures. *Nature*, **2019**, *567*, 71–75.

(37) Jin, C.; Regan, E.C.; Yan, A.; Iqbal Bakti Utama, M.; Wang, D.; Zhao, S.; Qin, Y.; Yang, S.; Zheng, Z.; Shi, S.; Watanabe, K.; Taniguchi, T.; Tongay, S.; Zettl, A.; Wang, F. *Nature*, **2019**, *567*, 76–80.

(38) Alexeev, E. M.; Ruiz-Tijerina, D. A.; Danovich, M.; Hamer, M. J.; Terry, D. J.; Nayak, P. K.; Ahn, S.; Pak, S.; Lee, J.; Sohn, J. I.; Molas, M. R.; Koperski, M.; Watanabe, K.; Taniguchi, T.; Novoselov, K. S.; Gorbachev, R. V.; Shin, H.S.; Fal'ko, W. I.; Tartakovskii, A. I. Resonantly Hybridized Excitons in Moiré Superlattices in van der Waals Heterostructures. *Nature*, **2019**, *567*, 81–86.

(39) Dal Conte, S.; Trovatello, C.; Gadermaier, C.; Cerullo, G. Ultrafast Photophysics of 2D Semiconductors and Related Heterostructures. *Trends Chem.*, **2020**, *2*, 28–42.

(40) Wang, H.; Bang, J.; Sun, Y.; Liang, L.; West, D.; Meunier, V.; and Zhang, S. The Role of Collective Motion in the Ultrafast Charge Transfer in van der Waals Heterostructures. *Nat. Commun.*, **2016**, *7*, 11504.

(41) Li, L.; Long, R.; Prezhdo, O. V. Charge Separation and Recombination in Two-Dimensional MoS_2/WS_2: Time-Domain *Ab Initio* Modeling. *Chem. Mater.*, **2016**, *29*, 2466–2473.

(42) Long, R.; Prezhdo, O. V. Quantum Coherence Facilitates Efficient Charge Separation at a $MoS_2/MoSe_2$ van der Waals Junction. *Nano Lett.*, **2016**, *16*, 1996–2003.

(43) Zheng, Q.; Saidi, W. A.; Xie, Y.; Lan, Z.; Prezhdo, O. V.; Petek, H.; Zhao, J. Phonon-Assisted Ultrafast Charge Transfer at Van Der Waals Heterostructure Interface. *Nano Lett.*, **2017**, *17*, 6435–6442.

(44) Zhang, J.; Hong, H.; Lian, C.; Ma, W.; Xu, X.; Zhou, X.; Fu, H.; Liu, K.; Meng, S. Interlayer-State-Coupling Dependent Ultrafast Charge Transfer in MoS_2/WS_2 bilayers. *Adv. Sci.*, **2017**, *4*, 1700086.

(45) Zheng, Q.; Xie, Y.; Lan, Z.; Prezhdo, O. V.; Saidi, W. A.; Zhao, J. Phonon-Coupled Ultrafast Interlayer Charge Oscillation at van der Waals Heterostructure Interfaces. *Phys. Rev. B*, **2018**, *97*, 205417.

(46) Ovesen, S.; Brem, S.; Linderälv, C.; Kuisma, M.; Korn, T.; Erhart, P.; Selig, M.; Malic, M. Interlayer Exciton Dynamics in van der Waals Heterostructures. *Commun. Phys.*, **2019**, *2*, 23.

(47) Liu, J.; Zhang, X.; Lu, G. Excitonic Effect Drives Ultrafast Dynamics in van der Waals Heterostructures. *Nano Lett.*, **2020**, *20*, 4631–4637.

(48) Wang, Y.; Wang, Z.; Yao, W.; Liu, G.-B.; Yu, H. Interlayer Coupling in Commensurate

and Incommensurate Bilayer Structures of Transition-Metal Dichalcogenides. *Phys. Rev. B*, **2017**, *95*, 115429.

(49) Raja, A.; Chaves, A.; Yu, J.; Arefe, G.; Hill, H. M.; Rigosi, A. F.; Berkelbach, T. C.; Nagler, P.; Schüller, C.; Korn, T.; Nuckolls, C.; Hone, J.; Brus, L. E.; Heinz, T. F.; Reichman, D. R.; Chernikov, A. Coulomb Engineering of the Bandgap and Excitons in Two-Dimensional Materials. *Nat. Commun.*, **2017**, *8*, 15251.

(50) Pogna, E. A. A.; Marsili, M.; De Fazio, D.; Dal Conte, S.; Manzoni, C.; Sangalli, D.; Yoon, D.; Lombardo, A.; Ferrari, A. C.; Marini, A.; Cerullo, G.; Prezzi, D. Photo-Induced Bandgap Renormalization Governs the Ultrafast Response of Single-Layer MoS_2. *ACS Nano*, **2016**, *10*, 1182–1188.

(51) Cunningham, P. D.; Hanbicki, A. T.; McCreary, K. M.; Jonker, B. T. Photoinduced Bandgap Renormalization and Exciton Binding Energy Reduction in WS_2. *ACS Nano*, **2017**, *11*, 12601–12608.

(52) Zhou, H.; Zhao, Y.; Zhu, H. Dielectric Environment-Robust Ultrafast Charge Transfer Between Two Atomic Layers. *J. Phys. Chem. Lett.*, **2019**, 10, 150-155.

(53) Chernikov, A.; Ruppert, C.; Hill, H. M.; Rigosi, A. F.; Heinz, T. F. Population Inversion and Giant Bandgap Renormalization in Atomically thin WS_2 layers. *Nat. Photon.*, **2015**, *9*, 466–470.

(54) Craig, C. F.; Duncan, W. R.; and Prezhdo, O. V. Trajectory Surface Hopping in the Time-Dependent Kohn-Sham Approach For Electron-Nuclear Dynamics. *Phys. Rev. Lett.*, **2012**, 137, 163001.

(55) Jaeger, H. M.; Fischer, S.; Prezhdo, O. V. Decoherence-Induced Surface Hopping. *J. Chem. Phys.*, **2012**, 95, 22A545.

(56) Long, R.; Prezhdo, O. V.; Fang, W. Nonadiabatic Charge Dynamics in Novel Solar Cell Materials. *Wiley Interdiscip. Rev. Comput. Mol. Sci.*, **2017**, 7, 1-29.

(57) Zhang, F.; Li, W.; Dai, X. Q., Modulation of Electronic Structures of $MoSe_2/WSe_2$ Van Der Waals Heterostructure by External Electric Field. *Solid State Commun.*, **2017**, 266, 11-15.

(58) Terrones, H.; Lopez-Urias, F.; Terrones, M., Novel Hetero-Layered Materials with Tunable Direct Band Gaps by Sandwiching Different Metal Disulfides and Diselenides. *Sci. Rep.*, **2013**, 3, 1549.

(59) Li, L. Q.; Long, R.; Prezhdo, O. V., Charge Separation and Recombination in Two-Dimensional MoS_2/WS_2: Time-Domain Ab Initio Modeling. *Chem. Mater.*, **2017**, 29, 2466-2473.

(60) O'Brien, M.; McEvoy, N.; Hanlon, D.; Hallam, T.; Coleman, J. N.; Duesberg, G. S., Mapping of Low-Frequency Raman Modes in Cvd-Grown Transition Metal Dichalcogenides: Layer Number, Stacking Orientation and Resonant Effects. *Sci. Rep.*, **2016**, 6, 19476.

(61) Wang, H.; Zhang, C.; Rana, F. Ultrafast Dynamics of Defect-Assisted Electron-Hole Recombination in Monolayer MoS_2. *Nano Lett.*, **2015**, 15, 339–345.

(62) Zhang, X.-X.; You, Y.; Yang, S.; Zhao, F.; Heinz, T. F. Experimental Evidence for Dark Excitons in Monolayer WSe_2. *Phys. Rev. Lett.*, **2015**, 115, 257403.